PAN ARCHIVES OF ACOUSTICS
Vol. 41, No. 3, pp. 461–472 (2016)
Copyright © 2016 by PAN – IPPT
DOI: 10.1515/aoa-2016-0045

Acoustic Scattering of 3D Complex Systems Having Random Rough Surfaces by Scalar Integral Equations

Juan Antonio GUEL-TAPIA[(1)], Francisco VILLA-VILLA[(1)],
Alberto MENDOZA-SUÁREZ[(2)], Héctor PÉREZ-AGUILAR[(2)]

[(1)] *Centro de Investigaciones en Óptica*
Loma del Bosque 115, Lomas del Campestre, León, Guanajuato 37150, México

[(2)] *Facultad de Ciencias Físico Matemáticas*
Universidad Michoacana de San Nicolás de Hidalgo
Av. Francisco J. Mújica S/N, Morelia, Mich. 58030, México; e-mail: hiperezag@yahoo.com

(*received October 26, 2015; accepted March 8, 2016*)

We propose a numerical surface integral method to study complex acoustic systems, for interior and exterior problems. The method is based on a parametric representation in terms of the arc's lengths in curvilinear orthogonal coordinates. With this method, any geometry that involves quadric or higher order surfaces, irregular objects or even randomly rough surfaces can be considered. In order to validate the method, the modes in cubic, spherical and cylindrical cavities are calculated and compared to analytical results, which produced very good agreement. In addition, as examples, we calculated the scattering in the far field and the near field by an acoustic sphere and a cylindrical structure with a rough cross-section.

Keywords: integral equations; Helmholtz equation; acoustic scattering.

1. Introduction

Application of the boundary element method (BEM) based on surface integral equations (SIE) to determine the scattered fields in two-dimensional (2D) and three-dimensional (3D) systems, has been widely used in optics, the propagation of seismic waves, and acoustics in the past (Pointer *et al.*, 1998; Pedersen *et al.*, 1994; Iturarán-Viveros *et al.*, 2007; Burton, Miller, 1971; Ursell, 1973; Piscoya, Ochmann, 2014; Zaman, 2000; Tadeu *et al.*, 2001; Maradudin *et al.*, 1990; Mendoza-Suárez, Méndez, 1997; Li, Huang, 2011).

In acoustics, the 3D wave equation implies a scalar Helmholtz equation when considering the potential for the displacement vector field or the pressure as arguments. Hence, the wave equation in the stationary regime is the same as in the 2D case, but with important differences, since the Green's function and its normal derivative present higher-order singularities.

This fact complicates the numerical solution when considering a boundary element method (BEM), which in general implies the expansion of integrands in curvilinear patches. In the application of BEM to the 3D case, researchers have proposed a number of variants to the solution of the integral equations associated with the Helmholtz equation, see Refs. (Zaman, 2000; Tadeu *et al.*, 2001; Chowdhury *et al.*, 2004; Kirkup, 1998), and references therein.

In this work we propose a solution of the SIE using a parametric representation on the surface integrals in terms of the arc's length in a curvilinear system. This formulation involves in a natural way the orthonormal basis $\widehat{\mathbf{n}}$, $\widehat{\mathbf{t}}_u$, $\widehat{\mathbf{t}}_v$, which are the normal and tangent vectors in the coordinate directions (u, v) of a surface.

It is worth observing that although the formalism proposed in this work seems to be applicable only to surfaces with certain symmetric geometries, such as spheres, cylinders or parametric surfaces in general, this is just a particular class of problems that can be treated. As we will demonstrate below, to apply the method to a given system it would be sufficient if the vectorial quantities, such as the normal and the curvature vectors, can be associated with each point on the surface, at least numerically. Consequently the formalism can also be applied to irregular surfaces or surfaces that do not necessarily have an analytical representation.

When reviewing the published work concerned with the numerical treatment of integrands in the vicinity of the singularities of the Green's function, and its normal derivative, we can see that this information is not clearly accessible in the literature, except for a few papers (Jun *et al.*, 1985; Huacasi *et al.*, 2003). In this study we propose the use of a Taylor series expansion to treat the singularities of diagonal elements, given the explicit procedure and matrix elements. This method has proven to give excellent results in the electromagnetic case, where surface integrals with higher-order singularities are present (Tong, Chew, 2010; Hanninen *et al.*, 2006).

The proposed numerical method is indeed a BEM, since it implies the solution of integral equations and sampling of surfaces. In contrast to other methods that expand into a functional basis of the field and its normal derivative, our method can determine these functions directly. This is an important characteristic, given that the precision of a BEM is based on the use of the functional base which, in turn, depends on selecting the appropriate base. For irregular surfaces, such as random rough surfaces or those of fractal kind, it is difficult to choose an adequate basis. The proposed method does not depend on this kind of choice and is useful for treating both regular and irregular surfaces. Perhaps the most important feature of this method is its versatility for solving scattering problems (exterior problems), resonant modes in cavities (interior problems), and calculations of the band structures in infinite periodic systems like photonic crystals without demanding complex modifications. It is not common to find such a variety of applications with any other BEM method. Finally, the proposed method is a generalization to 3D of the extensive earlier work that we have published regarding the application of the integral method to rigorously solve problems in 2D (Mendoza-Suárez *et al.*, 2004; 2006; 2007; 2011; Pérez-Aguilar *et al.*, 2013; Mendoza-Suárez, Pérez-Aguilar, 2015).

2. Theory

Let us consider Navier's equation for the propagation of acoustic waves (Morse, Ingard, 1968)

$$\nabla(\nabla \cdot \mathbf{u}) + k^2 \mathbf{u} = -\mathbf{f}, \tag{1}$$

where $\mathbf{u}$ represents the displacement vector of the point in the medium defined by the position vector $\mathbf{r}$; assuming that $\mathbf{u}$ oscillates at a frequency ω, and $k = \omega/c_l$ is the magnitude of the wave vector, and c_l the longitudinal speed of the wave in the acoustic medium. The external force $\mathbf{f}$ acts as a source for the perturbation. In order to develop the integral formalism we assume the case when $\mathbf{f} = \mathbf{0}$.

Taking the curl of Eq. (1)

$$k^2 \nabla \times \mathbf{u} = -\boldsymbol{\nabla} \times [\nabla(\nabla \cdot \mathbf{u})] = \mathbf{0}. \tag{2}$$

This implies that

$$\mathbf{u} = \boldsymbol{\nabla}\psi. \tag{3}$$

Thus, Navier's equation is satisfied if the potential ψ satisfies the Helmholtz equation

$$\nabla^2 \psi + k^2 \psi = 0. \tag{4}$$

By considering a point source, placed at $\mathbf{r}'$

$$\nabla^2 G(\mathbf{r}, \mathbf{r}') + k^2 G(\mathbf{r}, \mathbf{r}') = -\delta(\mathbf{r} - \mathbf{r}'), \tag{5}$$

we can demonstrate that a solution to this equation will be

$$G(\mathbf{r}, \mathbf{r}') = \frac{e^{ikR}}{4\pi R}, \tag{6}$$

which is known as the Green's function for the 3D Helmholtz equation.

Using the 2nd Green's identity with Eqs. (5) and (4), we can obtain

$$\int_{S'} \left[G(\mathbf{r}, \mathbf{r}') \frac{\partial \psi(\mathbf{r}')}{\partial n'} - \psi(\mathbf{r}') \frac{\partial G(\mathbf{r}, \mathbf{r}')}{\partial n'} \right] \mathrm{d}S' = \psi(\mathbf{r})\theta(\mathbf{r}) - \psi^{\mathrm{inc}}(\mathbf{r}), \tag{7}$$

with

$$\theta(\mathbf{r}') = \begin{cases} 1 & \text{if} \quad \mathbf{r}' \in V_2 \\ 0 & \text{if} \quad \mathbf{r}' \notin V_2, \end{cases} \tag{8}$$

where $\psi^{\mathrm{inc}}(\mathbf{r})$ represents an incident field for this exterior problem, R is the magnitude of $\mathbf{R} = \mathbf{r} - \mathbf{r}'$ with

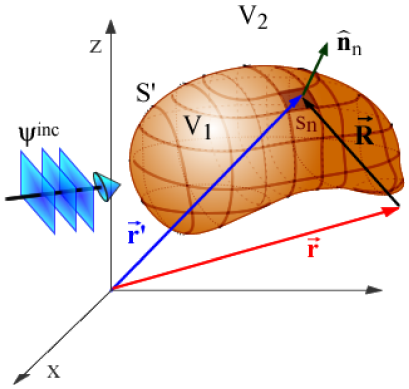

Fig. 1. Curvilinear system on a two-region geometry (interior and exterior problems). The observer's position is indicated by $\mathbf{r}$, while $\mathbf{r}'$ denotes the source position in the case of the differential equation, and the point on the surface for the integral surface equation. This vector spans the surface under integration.

$\mathbf{r}$ being the observer's position, and $\mathbf{r}'$ the integration vector that spans the surface S' (see Fig. 1), and

$$\frac{\partial G(\mathbf{r},\mathbf{r}')}{\partial n'} = \widehat{\mathbf{n}}\cdot\nabla' G(\mathbf{r},\mathbf{r}'), \\ = \gamma(\mathbf{r},\mathbf{r}')\,\widehat{\mathbf{n}}\cdot\mathbf{R}, \tag{9}$$

where $\widehat{\mathbf{n}}$ is the outward normal to the surface at $\mathbf{r}'$, and

$$\gamma(\mathbf{r},\mathbf{r}') = \frac{1}{4\pi}\left(R^{-3} - ikR^{-2}\right)e^{ikR}. \tag{10}$$

The potential and its normal derivative satisfy the boundary conditions on an interface

$$\psi^{(1)} = \psi^{(2)}, \qquad \frac{1}{\rho_1}\frac{\partial\psi^{(1)}}{\partial n'} = \frac{1}{\rho_2}\frac{\partial\psi^{(2)}}{\partial n'}, \tag{11}$$

where ρ_1 and ρ_2 represent the densities of the corresponding media. Sometimes, the conditions are given as (Burton, Miller, 1971)

$$\psi(\mathbf{r}') = f(\mathbf{r}'), \qquad \mathbf{r}'\in S', \quad \text{(Dirichlet)}, \tag{12}$$

$$\frac{\partial\psi}{\partial n'} = g(\mathbf{r}'), \qquad \mathbf{r}'\in S', \quad \text{(Neumann)}, \tag{13}$$

where $f(\mathbf{r}')$ and $g(\mathbf{r}')$ are arbitrary regular functions that define the corresponding boundary condition. To guarantee an outgoing scattered field, the Sommerfeld radiation condition,

$$\lim_{r\to\infty} r\left(\frac{\partial\psi}{\partial r} - ik\psi\right) = 0, \tag{14}$$

must be satisfied.

2.1. Integral equations: exterior and interior problems

Let us consider a closed surface S' that encloses the volume V_1, with an external incident scalar field impinging on it $\psi^{\text{inc}}(\mathbf{r})$ in region V_2 as shown in Fig. 1. By assuming that the normal points outward to S' and considering the convention that the surface integral is positive if the normal points outward and negative in the opposite case.

If we divide the surface into small surface elements S_n, which are rectangular regions, the integral equation for this medium will be

$$\sum_{n=1}^{N}\int_{S_n} G^{(2)}(\mathbf{r},\mathbf{r}')\frac{\partial\psi^{(2)}(\mathbf{r}')}{\partial n'}\,\mathrm{d}S' \\ -\sum_{n=1}^{N}\int_{S_n}\psi^{(2)}(\mathbf{r}')\frac{\partial G^{(2)}(\mathbf{r},\mathbf{r}')}{\partial n'}\,\mathrm{d}S' \\ = \psi^{(2)}(\mathbf{r}) - \psi^{\text{inc}}(\mathbf{r}). \tag{15}$$

In this equation, Green's function and its normal derivative are known and the potential $\psi(\mathbf{r}')$, and its normal derivative $\partial\psi(\mathbf{r}')/\partial n'$ constitute the functions to be determined. We have called these functions the source functions.

A similar equation holds for the case of an interior problem where V_1 is the region enclosed by the surface S' (normal outward) as

$$\sum_{n=1}^{N}\int_{S_n} G^{(1)}(\mathbf{r},\mathbf{r}')\frac{\partial\psi^{(1)}(\mathbf{r}')}{\partial n'}\,\mathrm{d}S' \\ -\sum_{n=1}^{N}\int_{S_n}\psi^{(1)}(\mathbf{r}')\frac{\partial G^{(1)}(\mathbf{r},\mathbf{r}')}{\partial n'}\,\mathrm{d}S' = 0. \tag{16}$$

We have added the upper index in parentheses to the functions in order to distinguish the problem when considering the properties of the acoustic medium in each case: ρ_1, k_1, and ρ_2, k_2, respectively.

If we assume that the surface elements are sufficiently small to guarantee that the potential and its normal derivative are approximately constant across S_n, then, the unknown functions can be taken out of the integrals to obtain

$$-\sum_{n=1}^{N}\Phi_n^{(2)}\int_{S_n} G^{(2)}(\mathbf{r},\mathbf{r}')\,\mathrm{d}S' \\ +\sum_{n=1}^{N}\psi_n^{(2)}\int_{S_n}\frac{\partial G^{(2)}(\mathbf{r},\mathbf{r}')}{\partial n'}\,\mathrm{d}S' \approx \psi^{\text{inc}}(\mathbf{r}), \tag{17}$$

in the case of an exterior problem or

$$\sum_{n=1}^{N}\Phi_n^{(1)}\int_{S_n} G^{(1)}(\mathbf{r},\mathbf{r}')\,\mathrm{d}S' \\ -\sum_{n=1}^{N}\psi_n^{(1)}\int_{S_n}\frac{\partial G^{(1)}(\mathbf{r},\mathbf{r}')}{\partial n'}\,\mathrm{d}S' \approx 0 \tag{18}$$

for the case of an interior problem. In both cases ($j = 1, 2$)

$$\psi_n^{(j)} = \psi^{(j)}(\mathbf{r}')\Big|_{\mathbf{r}'=\mathbf{r}_n}, \tag{19}$$

$$\Phi_n^{(j)} = \frac{\partial\psi^{(j)}(\mathbf{r}')}{\partial n'}\Big|_{\mathbf{r}'=\mathbf{r}_n}, \tag{20}$$

where $\mathbf{r}_n$ is a vector that points the centroid of S_n.

Integral equations for the source functions are obtained by letting $\mathbf{r} = \mathbf{r}'_m + \zeta\widehat{\mathbf{n}}_m$, where ζ is a positive infinitesimal and $m = 1, 2, ..., N$.

Let us consider a parametric representation of the integrals that appear in Eqs. (17) and (18) in terms of the arc's lengths s_u, and s_v (see Appendix). The parametrization can be expressed by the vector function, class C^2, $\mathbf{r}' = \mathbf{r}'(s_u, s_v)$. These arc's lengths correspond to the orthogonal directions of the curvilinear

system (orthogonal) proposed to represent the surfaces in question. Because of this fact the small surface elements, S_n, have a rectangular form, so $dS' = ds_u ds_v$. Such integrals define matrix elements, L_{mn} and N_{mn}, expressed as

$$L_{mn} = \lim_{\zeta\to 0^+} \int_{S_n} G(\mathbf{r},\mathbf{r}')|_{\mathbf{r}=\mathbf{r}'_m+\zeta\widehat{\mathbf{n}}_m}\, \mathrm{d}S'$$
$$= \lim_{\zeta\to 0^+} \int_{s_{v_n}-\frac{\Delta s_v}{2}}^{s_{v_n}+\frac{\Delta s_v}{2}} \int_{s_{u_n}-\frac{\Delta s_u}{2}}^{s_{u_n}+\frac{\Delta s_u}{2}} \cdot G(\mathbf{r},\mathbf{r}')|_{\mathbf{r}=\mathbf{r}'_m+\zeta\widehat{\mathbf{n}}_m}\, \mathrm{d}s_u\, \mathrm{d}s_v, \quad (21)$$

$$N_{mn} = \lim_{\zeta\to 0^+} \int_{S_n} \gamma(\mathbf{r},\mathbf{r}')\,\widehat{\mathbf{n}}(\mathbf{r}')\cdot(\mathbf{r}-\mathbf{r}')|_{\mathbf{r}=\mathbf{r}'_m+\zeta\widehat{\mathbf{n}}_m}\, \mathrm{d}S'$$
$$= \lim_{\zeta\to 0^+} \int_{s_{v_n}-\frac{\Delta s_v}{2}}^{s_{v_n}+\frac{\Delta s_v}{2}} \int_{s_{u_n}-\frac{\Delta s_u}{2}}^{s_{u_n}+\frac{\Delta s_u}{2}} \gamma(\mathbf{r},\mathbf{r}')\,\widehat{\mathbf{n}}(\mathbf{r}') \cdot(\mathbf{r}-\mathbf{r}')|_{\mathbf{r}=\mathbf{r}'_m+\zeta\widehat{\mathbf{n}}_m}\, \mathrm{d}s_u\, \mathrm{d}s_v. \quad (22)$$

The integration region involved in Eqs. (21) and (22) is shown in Fig. 2. The region is rectangular with a center point (s_{u_n}, s_{v_n}), and small length sides Δs_u and Δs_v.

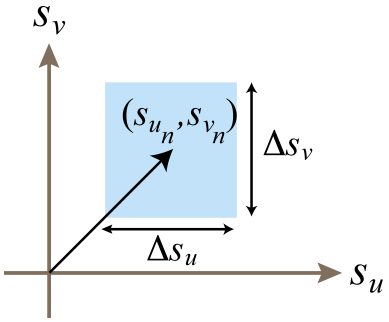

Fig. 2. Integration region involved in Eqs. (21) and (22).

In the case that $m \neq n$, the integrands possess no singularities for s_{u_n} and s_{v_n} within the range of integration. We can therefore approximate L_{mn} and N_{mn} by

$$L_{mn} \approx \frac{\Delta s^2}{4\pi}\frac{e^{ikR_{mn}}}{R_{mn}}, \quad (23)$$

$$N_{mn} \approx \frac{\Delta s^2}{4\pi}\frac{e^{ikR_{mn}}}{R_{mn}}\left(-\frac{1}{R_{mn}^2}+\frac{ik}{R_{mn}}\right)\widehat{\mathbf{n}}_n\cdot\mathbf{R}_{mn}, \quad (24)$$

where the vector $\mathbf{R}_{mn}$ is defined by $\mathbf{R}_{mn} = \mathbf{r}_m - \mathbf{r}_n$, its magnitude by $R_{mn} = |\mathbf{r}_m - \mathbf{r}_n|$ and we have assumed that $\Delta s_u = \Delta s_v = \Delta s$ for the sake of simplicity.

In evaluating the diagonal matrix elements, L_{nn} and N_{nn}, we have to take into account explicitly the singularities in the integrands of Eqs. (21) and (22) for coinciding arguments. Making the change of variables $\eta = s_u - s_{u_n}$, and $\xi = s_v - s_{v_n}$ leads to

$$L_{nn} = \lim_{\zeta\to 0^+} \int_{-\frac{\Delta s_v}{2}}^{\frac{\Delta s_v}{2}} \int_{-\frac{\Delta s_u}{2}}^{\frac{\Delta s_u}{2}} G(\mathbf{r},\mathbf{r}')|_{\mathbf{r}=\mathbf{r}'_n+\zeta\widehat{\mathbf{n}}_n}\, \mathrm{d}\eta\, \mathrm{d}\xi, \quad (25)$$

$$N_{nn} = \lim_{\zeta\to 0^+} \int_{-\frac{\Delta s_v}{2}}^{\frac{\Delta s_v}{2}} \int_{-\frac{\Delta s_u}{2}}^{\frac{\Delta s_u}{2}} \gamma(\mathbf{r},\mathbf{r}')\,\widehat{\mathbf{n}}(\mathbf{r}') \cdot(\mathbf{r}-\mathbf{r}')|_{\mathbf{r}=\mathbf{r}'_n+\zeta\widehat{\mathbf{n}}_n}\, \mathrm{d}\eta\, \mathrm{d}\xi. \quad (26)$$

Note that the variables η and ξ are small, thus the integrands can be expanded using the Taylor's power series.

Let us consider the position vector $\mathbf{r}'$ that denotes a point on the surface S'

$$\mathbf{r}'(s_u, s_v) = \mathbf{r}'(\eta + s_{u_n}, \xi + s_{v_n})$$
$$= \mathbf{r}'_n + \left.\frac{\partial \mathbf{r}'}{\partial \eta}\right|_{\eta=0,\xi=0}\eta + \left.\frac{\partial \mathbf{r}'}{\partial \xi}\right|_{\eta=0,\xi=0}\xi + \frac{1}{2}\left.\frac{\partial^2 \mathbf{r}'}{\partial \eta^2}\right|_{\eta=0,\xi=0}\eta^2 + \frac{1}{2}\left.\frac{\partial^2 \mathbf{r}'}{\partial \xi^2}\right|_{\eta=0,\xi=0}\xi^2 + \frac{1}{2}\left.\frac{\partial^2 \mathbf{r}'}{\partial \eta\partial \xi}\right|_{\eta=0,\xi=0}\eta\xi + \frac{1}{2}\left.\frac{\partial^2 \mathbf{r}'}{\partial \xi\partial \eta}\right|_{\eta=0,\xi=0}\xi\eta + \ldots, \quad (27)$$

expanded in a Taylor's series around the point $\mathbf{r}'_n$.

Because $\partial\mathbf{r}'/\partial\eta|_{\eta=0,\xi=0} = \partial\mathbf{r}'/\partial s_u|_{s_{u_n},s_{v_n}}$ and $\partial\mathbf{r}'/\partial\xi|_{\eta=0,\xi=0} = \partial\mathbf{r}'/\partial s_v|_{s_{u_n},s_{v_n}}$, we can identify from the differential geometry, the tangent vectors to the surface S',

$$\widehat{\mathbf{t}}_{u_n} = \widehat{\mathbf{t}}_u\Big|_{s_{u_n},s_{v_n}} = \left.\frac{\partial \mathbf{r}'}{\partial s_u}\right|_{s_{u_n},s_{v_n}} = \left.\frac{\partial \mathbf{r}'}{\partial \eta}\right|_{\eta=0,\xi=0}, \quad (28)$$

$$\widehat{\mathbf{t}}_{v_n} = \widehat{\mathbf{t}}_v\Big|_{s_{u_n},s_{v_n}} = \left.\frac{\partial \mathbf{r}'}{\partial s_v}\right|_{s_{u_n},s_{v_n}} = \left.\frac{\partial \mathbf{r}'}{\partial \xi}\right|_{\eta=0,\xi=0}, \quad (29)$$

and the curvature vectors, respectively

$$\mathbf{t}'_{u_n} = \left.\frac{\partial^2 \mathbf{r}'}{\partial s_u^2}\right|_{s_{u_n},s_{v_n}} = \left.\frac{\partial^2 \mathbf{r}'}{\partial \eta^2}\right|_{\eta=0,\xi=0}, \quad (30)$$

$$\mathbf{t}'_{v_n} = \left.\frac{\partial^2 \mathbf{r}'}{\partial s_v^2}\right|_{s_{u_n},s_{v_n}} = \left.\frac{\partial^2 \mathbf{r}'}{\partial \xi^2}\right|_{\eta=0,\xi=0}, \quad (31)$$

which in general are not unitary. These vectors are illustrated in Fig. 3 for a spherical surface.

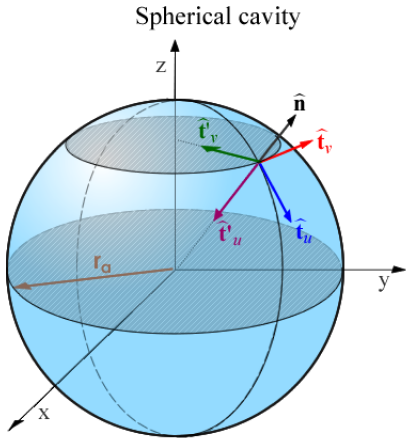

Fig. 3. Basis curvilinear vectors on a spherical parametric surface and their first derivatives.

We will define by shorthand notation, the vectors

$$\mathbf{t}'_{uv_n} = \left.\frac{\partial^2 \mathbf{r}'}{\partial s_u \partial s_v}\right|_{s_{u_n}, s_{v_n}} = \left.\frac{\partial^2 \mathbf{r}'}{\partial \eta \partial \xi}\right|_{\eta=0,\xi=0}, \quad (32)$$

$$\mathbf{t}'_{vu_n} = \left.\frac{\partial^2 \mathbf{r}'}{\partial s_v \partial s_u}\right|_{s_{u_n}, s_{v_n}} = \left.\frac{\partial^2 \mathbf{r}'}{\partial \xi \partial \eta}\right|_{\eta=0,\xi=0}. \quad (33)$$

Then, we can express the Eq. (27) to a first-order approximation

$$\mathbf{r}' \approx \mathbf{r}'_n + \hat{\mathbf{t}}_{u_n}\eta + \hat{\mathbf{t}}_{v_n}\xi + ... \quad (34)$$

In this way, the vector

$$\mathbf{R} = \mathbf{r} - \mathbf{r}' \approx \zeta\hat{\mathbf{n}}_n - \eta\hat{\mathbf{t}}_{u_n} - \xi\hat{\mathbf{t}}_{v_n}, \quad (35)$$

where the tangent vectors $\hat{\mathbf{t}}_{u_n}$, $\hat{\mathbf{t}}_{v_n}$, and the normal $\hat{\mathbf{n}}_n$ constitute a right hand set orthonormal basis. With these considerations, the magnitude of this vector, R, is given by

$$R \approx \left(\zeta^2 + \eta^2 + \xi^2\right)^{1/2}. \quad (36)$$

If we now consider the expansion of the tangent vectors around $\mathbf{r}_n$ up to first order

$$\hat{\mathbf{t}}_u = \hat{\mathbf{t}}_{u_n} + \mathbf{t}'_{u_n}\eta + \mathbf{t}'_{uv_n}\xi + ..., \quad (37)$$

$$\hat{\mathbf{t}}_v = \hat{\mathbf{t}}_{v_n} + \mathbf{t}'_{v_n}\xi + \mathbf{t}'_{vu_n}\eta + ..., \quad (38)$$

the normal vector can be expressed to a first order approximation as

$$\hat{\mathbf{n}} = \hat{\mathbf{t}}_u \times \hat{\mathbf{t}}_v \quad (39)$$

$$\approx (1 - \tau_{uv}\eta - \tau_{vu}\xi)\,\hat{\mathbf{n}}_n + (-\tau_{nu}\eta + \tau_{un}\xi)\,\hat{\mathbf{t}}_{u_n} + (-\tau_{nv}\xi + \tau_{un}\eta)\,\hat{\mathbf{t}}_{v_n}, \quad (40)$$

where the factors τ_{ij}, with $i, j = u, v, n$ have been defined in the Appendix. It is worth noticing that these factors, which involve dot products of basis vectors and their first derivatives, must be evaluated at point $\mathbf{r}'_n$.

With these results, we can calculate the product

$$\hat{\mathbf{n}}\cdot\mathbf{R} \approx \zeta - \zeta\tau_{uv}\eta - \zeta\tau_{vu}\xi - \tau_{un}\eta\xi + \tau_{nu}\eta^2 + \tau_{nv}\xi^2, \quad (41)$$

that appears in one of the integrands.

Now, let us consider Taylor's expansion of the exponential function present in Green's function

$$G(R) = \frac{1}{4\pi}\frac{\exp(ikR)}{R} = \frac{1}{4\pi}\sum_{m=0}^{\infty}\frac{(ik)^m}{m!}R^{m-1}. \quad (42)$$

In a similar fashion,

$$\gamma(R) = \frac{1}{4\pi}\sum_{m=0}^{\infty}\frac{1-m}{m!}(ik)^m R^{m-3}. \quad (43)$$

With these results, the integrals that constitute the diagonal matrix elements, $m = n$, can be calculated directly, obtaining

$$L_{nn} \approx \frac{\Delta s}{4\pi}\left[2\ln\left(\frac{1+\sqrt{2}}{1-\sqrt{2}}\right) + ik^2\Delta s\right], \quad (44)$$

$$N_{nn} \approx \frac{1}{2} + \frac{\Delta s}{4\pi}(\tau_{nu}+\tau_{nv})\left[\ln\left(\frac{1+\sqrt{2}}{1-\sqrt{2}}\right) + \frac{ik^3}{3}\Delta s\right]. \quad (45)$$

The matrix elements were expressed up to quadratic terms of the small parameter Δs and the factors τ_{nu} and τ_{nv}, which depend on the curvature vectors (see Appendix) given by $\hat{\mathbf{n}}_n \cdot \partial^2\mathbf{r}'/\partial s_u^2\big|_{s_{u_n}, s_{v_n}}$ and $\hat{\mathbf{n}}_n \cdot \partial^2\mathbf{r}'/\partial s_v^2\big|_{s_{u_n}, s_{v_n}}$, respectively. The Eqs. (23), (24) and (44), (45) give the matrix elements for any choice of the indices m and n.

3. Resonant modes in cubic and spherical cavities

To validate the method, let us consider a couple of problems that involve two different cavities with two types of surfaces that imply different types of boundary conditions. One condition is for perfectly soft surfaces and the other for perfectly hard surfaces. In both cases, we can use Eq. (18), to obtain a homogeneous algebraic linear system

$$\sum_{n=1}^{N} L_{mn}^{(1)}\Phi_n^{(1)} - \sum_{n=1}^{N} N_{mn}^{(1)}\psi_n^{(1)} = 0. \quad (46)$$

In the case of some regular surfaces, the curvilinear coordinates to be used are well-known, but it is important to mention that although an irregular surface cannot be modeled with curvilinear coordinates explicitly, the construction of orthonormal vector triads at each point of the surface is completely possible. An important fact when we consider a small vicinity on the surface is that this is approximately plane (see the schematic construction in Fig. 2). Therefore, even in the case of irregular surfaces, the proposed formalism

does not lose its applicability, and the most relevant feature relies on the form of the factors τ_{nu} and τ_{nv} in the matrix elements given by Eq. (45). Let us recall that, for example, according to Eqs. (82) and (84) of Appendix,

$$\tau_{nu} = \widehat{\mathbf{n}}_n \cdot \mathbf{t}'_{u_n} = \left(\left.\frac{\partial \mathbf{r}'}{\partial s_u}\right|_{s_{un},s_{vn}} \times \left.\frac{\partial \mathbf{r}'}{\partial s_v}\right|_{s_{un},s_{vn}} \right) \cdot \left.\frac{\partial^2 \mathbf{r}'}{\partial s_u^2}\right|_{s_{un},s_{vn}}, \quad (47)$$

which gives us a relation between the curvilinear vectors of the basis that can be defined at each point, even in the case of irregular surfaces. When considering an irregular surface, we necessarily know a number of points that are sufficient to represent such a surface, or perhaps we could use some computational algorithm to generate the surface in such a way that it is always possible to visualize it in 3D. We can assume that in some way we know the Cartesian coordinates of every point; so, we can apply a proper numerical procedure to such irregular geometry in order to define small surface elements S_n (assumed to be plane) and choose two mutually-orthogonal directions denoted by the directions s_u and s_v. A differential of arc in each direction would be equal to the magnitude of the differential change of $d\mathbf{r}'$ in each one of these directions. As a result, $\partial \mathbf{r}'/\partial s_u|_{s_{un},s_{vn}}$ and $\partial \mathbf{r}'/\partial s_v|_{s_{un},s_{vn}}$ are perpendicular unitary vectors. The vector $\mathbf{r}'$ can be represented in a parametric form by means of the Cartesian components, $x'(s_u, s_v)$, $y'(s_u, s_v)$, $z'(s_u, s_v)$. This is useful since, for example, $\partial \mathbf{r}'/\partial s_u$ can be calculated approximately with the simple formula $\partial \mathbf{r}'/\partial s_u \approx \Delta \mathbf{r}'/\Delta s_u = (\Delta x'/\Delta s_u, \Delta y'/\Delta s_u, \Delta z'/\Delta s_u)$, where in particular $\Delta x'/\Delta s_u \approx \Delta x'/\sqrt{\Delta x'^2 + \Delta y'^2 + \Delta z'^2}$, can be determined by knowing what the associated direction to s_u is, and using couples of points that determine the variation $\Delta \mathbf{r}'$. By following a similar procedure, it is possible to calculate numerically the second derivatives of $\mathbf{r}'$ with respect to the the arc's lengths s_u and s_v. With these expressions it is possible to obtain the matrix elements given in Eqs. (23), (24) and (44), (45). Let us clarify that in the numerical calculations that we performed to find the derivatives numerically, we took into account enough points (more than two) to obtain calculations with good accuracy.

It is not easy to obtain the matrix elements, L_{mn} and N_{mn}, in the case of diagonal elements; thus it is necessary to use a procedure to test them. This consists in analyzing the modes in cavities with symmetric geometry.

For a perfectly soft surface, the Dirichlet boundary condition $\psi(\mathbf{r}')|_{\mathbf{r}' \in S'} = 0$ cancels the second term of Eq. (46). This allows us to analyze and set up directly only these matrix elements

$$\sum_{n=1}^{N} L_{mn}^{(1)} \Phi_n^{(1)} = 0. \quad (48)$$

By solving the homogeneous linear system, it can be shown that the modes of the cavity can be calculated by finding the minimal of the determinant (Mendoza-Suárez *et al.*, 2006),

$$\Delta(\omega) = \ln\left(\left|\det L_{mn}^{(1)}\right|\right). \quad (49)$$

On the other hand, for a perfectly hard surface the Neumann boundary condition $\left(\Phi(\mathbf{r}')|_{\mathbf{r}' \in S'} = 0\right)$ cancels the first term of Eq. (46), and our system of equation transforms to

$$\sum_{n=1}^{N} N_{mn}^{(1)} \psi_n^{(1)} = 0. \quad (50)$$

This procedure allows us to check the complementary matrix elements $N_{mn}^{(1)}$ independently, following a similar criterion by finding the minimum of the determinant,

$$\Delta(\omega) = \ln\left(\left|\det N_{mn}^{(1)}\right|\right). \quad (51)$$

The cavities chosen are a cube and a sphere, where the Helmholtz equation has analytical solutions. In the case of a cubic cavity with edges of length D, and one corner at the origin of a Cartesian system of coordinates, solving the Helmholtz equation allow us to demonstrate that the frequencies spectrum can be obtained from the relation

$$k = \frac{\omega}{c_l} = \frac{\pi}{D}\left(l^2 + m^2 + n^2\right)^{1/2}, \quad (52)$$

where k is the magnitude of the wave vector as before, and l, m, and n are the numbers $1, 2, 3, ...$ when considering the Dirichlet boundary conditions

$$\psi(0, y, z) = \psi(D, y, z) = 0, \quad (53)$$

$$\psi(x, 0, z) = \psi(x, D, z) = 0, \quad (54)$$

$$\psi(x, y, 0) = \psi(x, y, D) = 0. \quad (55)$$

When the Neumann boundary conditions are

$$\left.\frac{\partial \psi}{\partial n'}\right|_{(0,y,z)} = \left.\frac{\partial \psi}{\partial n'}\right|_{(D,y,z)} = 0, \quad (56)$$

$$\left.\frac{\partial \psi}{\partial n'}\right|_{(x,0,z)} = \left.\frac{\partial \psi}{\partial n'}\right|_{(x,D,z)} = 0, \quad (57)$$

$$\left.\frac{\partial \psi}{\partial n'}\right|_{(x,y,0)} = \left.\frac{\partial \psi}{\partial n'}\right|_{(0,y,D)} = 0, \quad (58)$$

the parameters are $l, m, n = 0, 1, 2, ...$

Expressing the frequency in reduced units $\omega = \overline{\omega} 2\pi c_l/D$, considering D as a normalization parameter in this case, solving for the reduced frequency spectrum for a cubic cavity will be

$$\overline{\omega} = \frac{1}{2}\left(l^2 + m^2 + n^2\right)^{1/2}. \quad (59)$$

It is important to note that in both cases, the position of the modes in the reduced frequency scheme are independent of the size of the cavity. This is quite convenient while testing the programed algorithms.

We can show that when the cavity is spherical, it is also possible to obtain an analytical relation (Arfken *et al.*, 2013)

$$\overline{\omega} = \frac{\alpha_{li}}{2\pi}, \tag{60}$$

where we have taken the radius of the sphere r_a as a normalization parameter in this case. α_{l_i} represents the i-th zero of the spherical Bessel functions of order l when the boundary conditions are those stated in Eq. (53). The first zeros of these functions are $\alpha_{01} = \pi$, $\alpha_{02} = 2\pi$, $\alpha_{11} = 4.4934$, $\alpha_{12} = 7.7253$, $\alpha_{21} = 5.7635$, $\alpha_{22} = 9.0950$, $\alpha_{30} = 6.9879$,...

When the derivative of the scalar field is involved, the boundary conditions that have to be considered are those given in Eq. (57). These conditions imply that these modes are given in terms of the zeros of the first derivative of the spherical Bessel functions $\alpha_{11} = 2.0816$, $\alpha_{21} = 3.3421$, $\alpha_{01} = 4.4934$, $\alpha_{31} = 4.5141$, $\alpha_{41} = 5.6467$, $\alpha_{12} = 5.9404$,...

It is important to observe that the cubic cavity allows us to analyze in detail each integral separately from the corresponding boundary conditions in each case, since the terms involving the curvatures are zero $\tau_{nu} = \tau_{nv} = 0$. On the other hand, when considering the spherical cavity, in addition to the terms of the expansion already considered, the terms that involving the curvatures τ_{nu}, τ_{nv} come to play an important role in the matrix elements $N^{(1)}_{mn}$.

In Table 1, we compare the modes position for a cubic cavity and a spherical cavity of radius r_a, analytically- and numerically-determined for $L^{(1)}_{mn}$ and $N^{(1)}_{mn}$, respectively, which are in very good agreement. In this calculation, $\Delta s \approx D/10$ was considered.

Table 1. Eigenfrequencies of cubic and spherical cavities calculated analytically ($\overline{\omega}_a$) and numerically ($\overline{\omega}_{L_{mn}}$ and $\overline{\omega}_{N_{mn}}$) expressed in reduced units $\overline{\omega}$.

Cubic Cavity						
$\psi(\mathbf{r}')\|_{\mathbf{r}'\in S'} = 0$						
$\overline{\omega}_a$	0.866	1.225	1.500	1.658	1.732	1.871
$\overline{\omega}_{L_{mn}}$	0.872	1.230	1.507	1.669	1.742	1.881
$\Phi(\mathbf{r}')\|_{\mathbf{r}'\in S'} = 0$						
$\overline{\omega}_a$	0.000	0.500	0.707	0.866	1.000	1.118
$\overline{\omega}_{N_{mn}}$	0.027	0.505	0.712	0.872	1.003	1.123
Spherical Cavity						
$\psi(\mathbf{r}')\|_{\mathbf{r}'\in S'} = 0$						
$\overline{\omega}_a$	0.500	0.715	0.917	1.000	1.112	1.230
$\overline{\omega}_{L_{mn}}$	0.502	0.719	0.921	1.069	1.116	1.234
$\Phi(\mathbf{r}')\|_{\mathbf{r}'\in S'} = 0$						
$\overline{\omega}_a$	0.331	0.532	0.715	0.718	0.899	0.945
$\overline{\omega}_{N_{mn}}$	0.333	0.532	0.719	0.719	0.897	0.943

4. Resonant modes in cylindrical cavities with a rough cross-section

The examples considered up to this point imply the application of our numerical method to smooth surfaces with a regular and well-defined geometry. However, we can go further by showing that the method is useful for treating problems involving cavities with random surfaces as well.

Let us state that a rough surface can be modeled by creating ensembles of numerically-generated specific contours (Maradudin *et al.*, 1990; Mendoza-Suárez *et al.*, 2004). Each one of these contours is usually known as a realization. Figure 4 represents a cylindrical cavity with a cross-section given by a realization of the ensemble (curved wall) and flat faces. We calculated some acoustic modes assuming that the Dirichlet boundary condition is satisfied on the surface S: $\psi|_S = 0$.

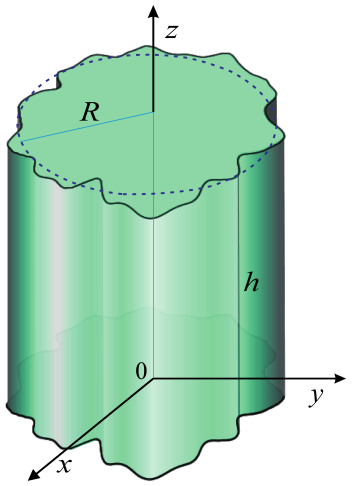

Fig. 4. Cylindrical cavity with a rough cross-section.

To calculate the matrix elements for this structure we have chosen the direction s_u to be tangent to the profile assigned to the realization shown, and the direction s_v was taken along the z direction. In addition, it is necessary to assume that such a realization can be represented by a continuous function with continuous derivatives up to the second order. From a practical point of view, we obtain realizations of the random surface using discrete sets of points. These sets satisfy the proper conditions to allow the numerical calculation of the derivatives of the profiles. The plot representations of these profiles with sufficient points appear as C^2 class curves.

The statistical properties of the modeled rough curved wall profile employed in this work can be found

in Mendoza-Suárez *et al.* (2004). Let $r(\theta)$ be a function that represents the general required profile with $0 \leq \theta < 2\pi$, defined in terms of the statistical properties as given below.

The average profile is a circumference of radius R,

$$\langle r(\theta) \rangle = R. \tag{61}$$

We can define the function

$$\delta r(\theta) = r(\theta) - R, \tag{62}$$

where $\delta r(\theta)$ represents the radial fluctuations of the profile with respect to the reference circumference. The curved wall can be modeled by a Gaussian probability density function, given by

$$f(\delta r) = \left(1/\sqrt{2\pi}\sigma\right) \exp\left(-\frac{(\delta r)^2}{2\sigma^2}\right), \tag{63}$$

where σ represents the standard deviation of heights of the surface roughness.

We also define the angular correlation function,

$$B(\theta, \theta') = \frac{1}{\sigma^2} \langle \delta r(\theta) \delta r(\theta') \rangle, \tag{64}$$

by assuming that it has a Gaussian form

$$B(\theta, \theta') = B(|\theta - \theta'|) \exp\left(-\frac{(\theta - \theta')^2}{\Theta^2}\right), \tag{65}$$

where Θ is the "angular correlation length", which represents the angular scale of the random roughness.

For any problem involving a cavity the random rough profiles must close onto itself. Thus, the first and last points of a realization, are ideally neighbor points that are correlated. To consider this fact, we use a linear relation given by

$$\delta r(\theta_k) = \sigma \sum_{j=-\infty}^{\infty} \omega_j X_{j+k}, \tag{66}$$

where ω_j is a set of undetermined weights and X_j is a Gaussian independent variable that form an infinite periodic sequence satisfying the relation given by $\langle X_i X_j \rangle = \delta_{ij+nN}$ for $n = 0, \pm 1, \pm 2, \ldots$ The periodicity of this sequence is the key point to adequately finding closed- and correlated-realizations. Obtaining the weights by a Fourier transformation (see Ref. (Mendoza-Suárez *et al.*, 2004)) and using Eq. (66), we obtain

$$\delta r(\theta_k) = \sigma \sum_{j=-\infty}^{\infty} \left(\frac{2\Delta\theta}{\Theta\sqrt{\pi}}\right)^{1/2} \cdot \exp\left(-\frac{2(\Delta\theta)^2 (j - nN)^2}{\Theta^2}\right) X_{j+k}, \tag{67}$$

where $\Delta\theta$ is the angular separation between consecutive angles. From the last expression, we can find values for $\delta r(\theta)$, and finally an ensemble of profiles with the required statistical properties.

The parameters used to generate the surface profiles of our system for a curved wall with random roughness were $R = 4$, $\Theta = 10°$ and $\sigma = R/10$ (R in arbitrary units), which correspond to a small roughness amplitude. The cylindrical structure has a height of $h = \pi$. The realizations were calculated using Eq. (67), with $n = 0$, and the number of points considered in one realization was $N = 360$ with a constant angular separation of $\Delta\theta = 1°$. The eigenvalue spectra and intensity patterns for one realization were compared to the corresponding spectra for a perfectly circular profile. Figure 5 shows the result of the numerical calculation for the normalized intensity distribution of the first (Fig. 5a) and second (Fig. 5b) state for the circular profile considered for the eigenvalues $\omega_1 = 1.1829$ and $\omega_2 = 1.4022$, respectively. For the realization considered, the intensity computed is shown in Fig. 5c for the first state and in Fig. 5d for the second state with the eigenvalues $\omega_1 = 1.1836$ and $\omega_2 = 1.3877$, respectively. The normalized intensities were calculated on a plane perpendicular to the axis of the cylinder that was divided into two equal parts.

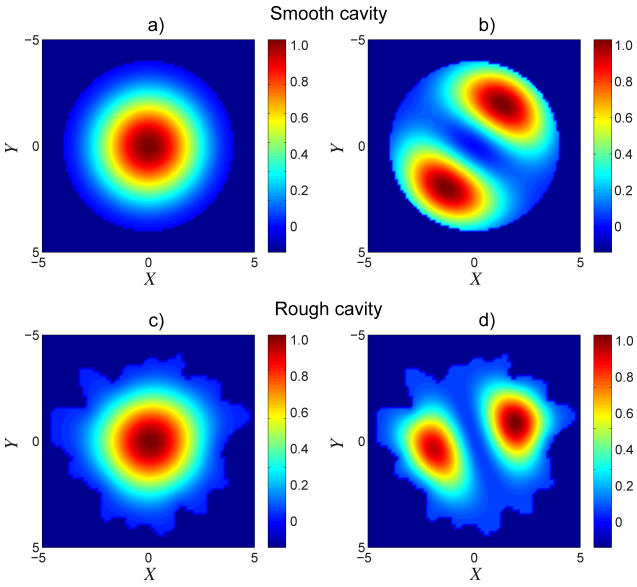

Fig. 5. Normalized intensity of the a) first and b) second state for the perfectly circular profile. Normalized intensity of the c) first and d) second state for the surface profile with random wall roughness.

We observed that this numerically calculated intensity distribution for the first state still conserves the symmetry with a small wall roughness (Fig. 5a and 5c). However, for the second state we can observe that the effect of roughness has changed the orientation of the non-symmetrical mode (Fig. 5d). Although in this paper we only show results for one realization, in Ref. (Mendoza-Suárez *et al.*, 2004) a similar system is shown with more detail to demonstrate how the aver-

aged intensity on an ensemble of samples results in an almost radially symmetric pattern, with a practically null angular dependence.

5. Scattering by a sphere and a cylindrical structure

Now that the method has been validated, let us calculate the scattering of a rigid acoustic sphere and a cylindrical structure with a rough cross-section, when an incident scalar field excites the system. In this case, Eq. (17) can be expressed as

$$-\sum_{n=1}^{N} L_{mn}^{(2)} \Phi_n^{(2)} + \sum_{n=1}^{N} N_{mn}^{(2)} \psi_n^{(2)} = \psi_m^{\text{inc}}, \qquad (68)$$

where we have called $\psi_m^{\text{inc}} = \psi^{\text{inc}}(\mathbf{r}_m)$. The incident wave represents a plane wave traveling along the positive direction of the x-axis, as shown in Fig. 1. If we represent the vector $\mathbf{r}$ in Cartesian coordinates, then

$$\psi^{\text{inc}}(x, y, z) = e^{ik_2 x}. \qquad (69)$$

Considering the case of acoustic surfaces that are perfectly soft or perfectly hard, we have the Dirichlet boundary condition, $\psi_n^{(2)} = 0$, and the Neumann boundary condition, $\Phi_n^{(2)} = 0$, respectively. In each case the Eq. (68) reduces to an inhomogeneous system of linear equations; so by solving this linear system, the source functions, $\Phi_n^{(2)}$ and $\psi_n^{(2)}$, can be determined for a set of points r'_n on the surface S'.

Once these sources are obtained, the field at any point $\mathbf{r}$ outside the scattering system can be calculated using Eq. (7), as will be shown in the following section.

5.1. The near field and far field: Dirichlet and Neumann boundary conditions

For the exterior problem we can find numerical expressions for the field $\psi(\mathbf{r})$, at any observation point $\mathbf{r}$, whenever this point lies at least infinitesimally outside the surface S'.

Let us consider first the Dirichlet boundary condition given in Eq. (12) with $f(\mathbf{r}') = 0$. From Eqs. (6), (7) and (20) we obtain the expression

$$\begin{aligned} \psi_{\text{scat}}(\mathbf{r}) &\equiv \psi(\mathbf{r}) - \psi^{\text{inc}}(\mathbf{r}) \\ &= \frac{1}{4\pi} \int_{S'} \frac{e^{ik_2 R}}{R} \Phi(\mathbf{r}')\, dS', \end{aligned} \qquad (70)$$

where $R = |\mathbf{r} - \mathbf{r}'|$ and $\psi_{\text{scat}}(\mathbf{r})$ represents the scattered field. Expressing the vectors $\mathbf{r}$ and $\mathbf{r}'$ in terms of their Cartesian components, the scattered field can be approximated numerically by

$$\psi_{\text{scat}}(x, y, z) = \sum_{n=1}^{N} \frac{\Delta s^2}{4\pi} \frac{e^{ik_2\sqrt{a^*}}}{\sqrt{a^*}} \Phi_n^{(2)}, \qquad (71)$$

where

$$a^* = (x - x'_n)^2 + (y - y'_n)^2 + (z - z'_n)^2.$$

In this equation we assume that $\Phi_n^{(2)}$ has already been determined by the solution of the linear system given in Eq. (68). With this expression, the field at any distance from the scattering surface can be calculated, including any point lying in the near field. In addition, we define the scattering intensity as $I(x, y, z) = |\psi_{\text{scat}}(x, y, z)|^2$.

In the case of the far field, let us consider that the observer's position $\mathbf{r}$ is far away from the scatterer system. That is $|\mathbf{r}| \gg |\mathbf{r}'_n|$ para $n = 1, 2, ..., N$. In this case, we can obtain the approximated expression

$$R = \sqrt{(\mathbf{r} - \mathbf{r}'_n) \cdot (\mathbf{r} - \mathbf{r}'_n)} \simeq r - \widehat{\mathbf{r}} \cdot \mathbf{r}'_n, \qquad (72)$$

for the denominator of Eq. (71), and this is sufficient to consider the first term on the right hand side of this equation. From Fig. 6

$$\mathbf{r}'_n = x'_n \widehat{\mathbf{i}} + y'_n \widehat{\mathbf{j}} + z'_n \widehat{\mathbf{k}}, \qquad (73)$$

$$\widehat{\mathbf{r}} = \sin\theta_s \widehat{\mathbf{j}} + \cos\theta_s \widehat{\mathbf{k}}, \qquad (74)$$

where θ_s is the scattering angle on the $y-z$ plane.

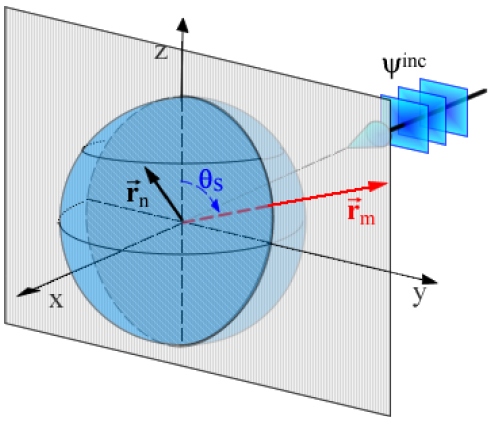

Fig. 6. Schematic description of far field geometry. θ_s represents the scattering angle of observation.

For the scattered far field, we obtain

$$\psi_{\text{scat}}(r, \theta_s) = \sigma(\theta_s) \frac{e^{ik_2 r}}{r},$$

where the angular scattering amplitude, $\sigma(\theta_s)$, is given by

$$\sigma(\theta_s) = \sum_{n=1}^{N} \frac{\Delta s^2}{4\pi} e^{-ik_2\left(y'_n \sin\theta_s + z'_n \cos\theta_s\right)} \Phi_n^{(2)},$$

and represents the angular behavior of the scattered wave in the far field. Also, we define the angular scattering intensity as $I(\theta_s) = |\sigma(\theta_s)|^2$.

Let us now consider the Neumann boundary condition given in Eq. (13). With $g(\mathbf{r}') = 0$, Eqs. (7), (9) and (10) produce

$$\psi_{\text{scat}}(\mathbf{r}) \equiv \psi(\mathbf{r}) - \psi^{\text{inc}}(\mathbf{r}) = \frac{1}{4\pi}\int_{S'} \frac{e^{ik_2 R}}{R} \cdot \left(\frac{1}{R^2} - \frac{ik_2}{R}\right) \widehat{\mathbf{n}}(\mathbf{r}') \cdot \mathbf{R}\psi^{(2)}(\mathbf{r})\, \mathrm{d}S'. \quad (75)$$

This integral can be calculated with the approximated expression

$$\psi_{\text{scat}}(x,y,z) = \sum_{n=1}^{N} \frac{\Delta s^2}{4\pi} \frac{e^{ik_2 R_n}}{R_n} \left(\frac{1}{R_n^2} - \frac{ik_2}{R_n}\right) \widehat{\mathbf{n}}_n \cdot \mathbf{R}_n \psi_n^{(2)},$$

where $\mathbf{R}_n = \mathbf{r} - \mathbf{r}'_n = (x - x'_n, y - y'_n, z - z'_n)$. The last equation allows us to obtain the scattered field at any distance from the scatterer having calculated $\psi_n^{(2)}$ from the linear system given in Eq. (68). The normal vector $\widehat{\mathbf{n}}_n$ can be determined at least numerically, even for irregular surfaces.

For the far scattered field we consider similar approximations to the previous case in addition for neglecting the term $1/R_n^2$, as is commonly done in radiation theory, obtaining in this case

$$\psi_{\text{scat}}(r, \theta_s) = \sigma(\theta_s) \frac{e^{ik_2 r}}{r},$$

where the dispersion amplitude $\sigma(\theta_s)$, can be calculated from

$$\sigma(\theta_s) = -\sum_{n=1}^{N} \frac{ik_2 \Delta s^2}{4\pi} e^{-ik_2\left(y'_n \sin\theta_s + z'_n \cos\theta_s\right)} \cdot \left(n_{y_n} \sin\theta_s + n_{z_n} \cos\theta_s\right) \psi_n^{(2)}.$$

The scattered far field calculated for the system composed of a rigid sphere of unit radius, $r_a = 1$, for three different values of the product $k_2 r_a = 2.0$, 4.0, 8.0, are shown in Fig. 7.

Figures 7a, 7b and 7c can be compared to the corresponding Ref. (Junger, Feit, 2004), obtaining good agreement. To solve the problem of spurious resonant modes, we implemented the method of the dual surface recently proposed by Piscoya and Ochmann (2014). This implies the construction of an auxiliary surface: a concentric sphere with a radius $r_b = r_a - \delta$, and the reformulation of the system of equations with a pure imaginary factor α. The parameters we considered were $\delta = \lambda/10$, and $\alpha = i$.

We considered another example of an exterior problem that involved a soft, randomly rough cylinder. We calculated the near field and the far field intensities for this irregular scattering surface, as shown in Fig. 4. The parameters used to generate the surface profiles of a cylindrical structure with a rough cross-section

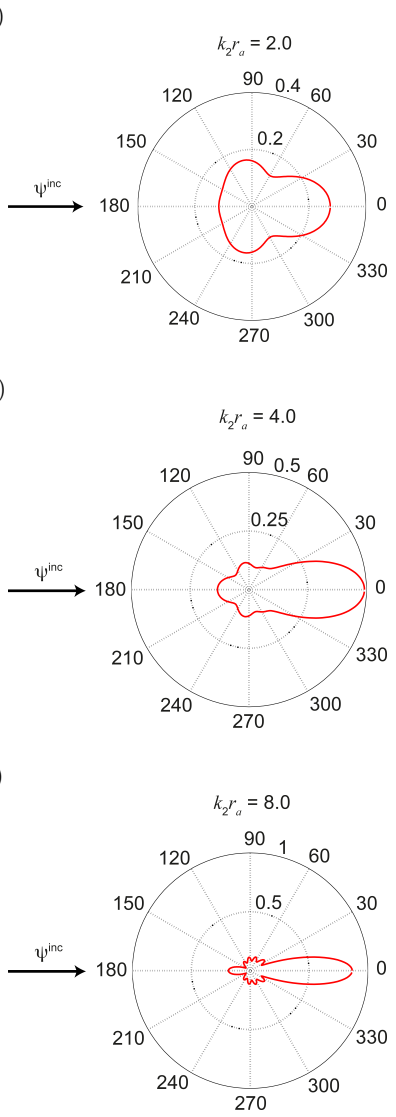

Fig. 7. Scattering intensity in the far field region for a rigid sphere of radius $r_a = 1.0$. The intensity is shown in a polar diagram, where the radius from the origin to the intersection of the curve represents the intensity as a function of θ_s on the y–z plane for: a) $k_2 r_a = 2.0$, b) $k_2 r_a = 4.0$, and c) $k_2 r_a = 8.0$.

were the same as in Fig. 5. The cylindrical structure is illuminated for an acoustic plane wave with unit amplitude $\psi^{\text{inc}}(\mathbf{r}) = e^{ikz}$. Figure 8 shows the scattering intensity (Fig. 8a) and the angular scattering intensity (Fig. 8b) on the plane $z = h/2$, where the height of the cylinder structure is $h = \pi$. As we hoped, the patterns do not have a symmetrical form. The important aspect of this example is that our method proved able to calculate near field or far field for regular or irregular scattering surfaces, without large changes. We only have to calculate the factor $(\tau_{nu} + \tau_{nv})$ in each case that appears in Eq. (45) to complete the calculation of the matrix elements of the system.

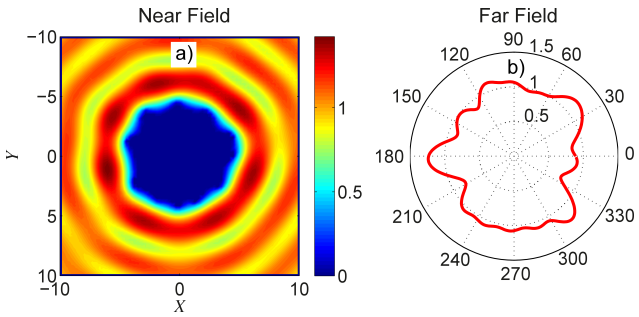

Fig. 8. a) Scattering intensity in the near field and b) angular scattering intensity in the far field region for a soft, randomly rough cylinder of radius $R = 4.0$. The scattering intensities are shown on the $x-y$ plane in half of the cylinder height.

6. Conclusions

We proposed a surface integral method to study acoustic systems for interior and exterior problems. The method is based on a parametric representation in terms of the arc's lengths in curvilinear orthogonal coordinates. The change in the magnitudes of tangent vectors are associated with the principal curvatures of the surfaces as important quantities that allow us to state a criterion for the proper partition of the surfaces by defining the differential arc's length along both principal directions, u and v. With this method, any geometry that involves quadric or higher order surfaces, irregular objects, or even randomly rough surfaces can be considered. To validate the method, the resonant modes in cubic and spherical cavities were calculated and compared to analytical results, finding very good agreement. Also, as examples, we calculated the scattering in the far field and the near field by an acoustic sphere and a cylindrical structure with a rough cross-section.

Appendix. Relations among the basis vectors and their derivatives

Let us consider the unit vector

$$\widehat{\mathbf{t}}_u \cdot \widehat{\mathbf{t}}_u = 1. \tag{76}$$

Differentiating this product

$$\frac{\partial\left(\widehat{\mathbf{t}}_u \cdot \widehat{\mathbf{t}}_u\right)}{\partial s_u} = 2\widehat{\mathbf{t}}_u \cdot \frac{\partial \widehat{\mathbf{t}}_u}{\partial s_u} = 0, \tag{77}$$

so, $\widehat{\mathbf{t}}_u \perp \mathbf{t}'_u$. In a similar way we can demonstrate that $\widehat{\mathbf{t}}_v \perp \mathbf{t}'_v$.

The normal vector at the point $\mathbf{r}_n$ is defined as

$$\widehat{\mathbf{n}}_n = \widehat{\mathbf{t}}_{u_n} \times \widehat{\mathbf{t}}_{v_n}. \tag{78}$$

As $\widehat{\mathbf{t}}_{u_n} \perp \mathbf{t}'_{u_n}$, then

$$\mathbf{t}'_{u_n} = \tau_{vu}\widehat{\mathbf{t}}_{v_n} + \tau_{nu}\widehat{\mathbf{n}}_n, \tag{79}$$

$$\mathbf{t}'_{v_n} = \tau_{uv}\widehat{\mathbf{t}}_{u_n} + \tau_{nv}\widehat{\mathbf{n}}_n, \tag{80}$$

where

$$\tau_{vu} = \widehat{\mathbf{t}}_{v_n} \cdot \mathbf{t}'_{u_n}, \tag{81}$$

$$\tau_{nu} = \widehat{\mathbf{n}}_n \cdot \mathbf{t}'_{u_n}, \tag{82}$$

$$\tau_{uv} = \widehat{\mathbf{t}}_{u_n} \cdot \mathbf{t}'_{v_n}, \tag{83}$$

$$\tau_{nv} = \widehat{\mathbf{n}}_n \cdot \mathbf{t}'_{v_n}. \tag{84}$$

Following similar lines, it can be shown that

$$\mathbf{t}_{uv_n} = -\tau_{vu}\widehat{\mathbf{t}}_{u_n} - \tau_{uv}\,\widehat{\mathbf{t}}_{v_n} - \tau_{un}\widehat{\mathbf{n}}_n, \tag{85}$$

where $\tau_{un} = \widehat{\mathbf{t}}_{u_n} \cdot \partial\widehat{\mathbf{n}}_n/\partial s_v$.

Acknowledgments

The authors A. Mendoza-Suárez and H. Pérez-Aguilar express their gratitude to the Coordinación de la Investigación Científica de la Universidad Michoacana de San Nicolás de Hidalgo, and PROMEP UMSNH-PTC-364 for the financial support granted for the development of this research project.

We are also indebted to Dr. Bernardo Mendoza and the authorities of the Centro de Investigaciones en Óptica for the partial support provided for this study by allowing access to the Medusa cluster.

References

1. Arfken G.B., Weber H.J., Harris F.E. (2013), *Mathematical Methods for Physicists*, 7th edition, Academic Press, USA.
2. Burton A.J., Miller G.F. (1971), *The application of integral equation methods to the numerical solution of some exterior boundary-value problems*, Proc. Roy. Soc. Lond., **323**, 201–210.
3. Chowdhury N.M.A., Takada J.I., Hirose M. (2004), *3D scalar-formulation of IE-MEI for acoustic scattering*, IEEE Conf. Antennas Propag. Soc. Int. Symp., **3**, 2251–2254.
4. Hanninen I., Taskinen M., Sarvas J. (2006), *Singularity substraction formulaes for surface integral equations with rwg, rooftop and hybrid basis functions*, Progr. Electromag. Res., **63**, 243–278.
5. Huacasi W., Mansur W.J., Azevedo J.P.S. (2003), *A novel hypersingular B.E.M. formulation for three-dimensional potential problems*, J. of the Braz. Soc. of Mech. Sci. & Eng., **25**, 364–372.
6. Iturarán-Viveros U., Sánchez-Sesna F.J., Luzón F. (2007), *Boundary element simulation of scattering of elastic waves by 3D cracks*, J. Appl. Gephys., **64**, 70–82.

7. Jun L., Beer G., Meek J.J. (1985), *Efficient evaluation of integrals of order* $1/r$, $1/r^2$, $1/r^3$ *using a gaussian quadrature*, Eng. Analysis, **2**, 118–123.
8. Junger M.C., Feit D. (2004), *Sound, structures, and their Interaction*, MIT Press, USA.
9. Kirkup S. (1998), *The boundary element method in acoustics*, Integrated Sound Software.
10. Li S., Huang Q. (2011), *A new fast multipole boundary element method for two-dimensional acoustic problems*, Comp. Meth. Appl. Mech. Eng., **200**, 1333–1340.
11. Maradudin A.A., Méndez E.R., Michel T. (1990), *Enhanced backscattering of light from a random grating*, Ann. Phys., **203**, 255–307.
12. Mendoza-Suárez A., Méndez E.R. (1977), *Light scattering by a reentrant fractal surface*, Appl. Opt., **36**, 3521–3531.
13. Mendoza-Suárez A., Pérez-Aguilar H. (2015), *Optical response of a photonic crystal waveguide that includes a dispersive left-handed material*, Photonic. Nanostruct., **14**, 93–100.
14. Mendoza-Suárez A., Corona U.R., Luna R.E. (2004), *Effects of wall random roughness on te and tm modes in a hollow conducting waveguide*, Opt. Commun., **238**, 291–299.
15. Mendoza-Suárez A., Villa-Villa F., Gaspar-Armenta J.A. (2006), *Numerical method based on the solution of integral equations for the calculation of the band structure and reflectance of one and two-dimensional photonic crystals*, J. Opt. Soc. Am. B, **23**, 2249–2256.
16. Mendoza-Suárez A., Villa-Villa F., Gaspar-Armenta J.A. (2007), *Band structure of two-dimensional photonic crystals that include dispersive left-handed materials and dielectrics in the unit cell*, J. Opt. Soc. Am. B, **24**, 3091–3098.
17. Mendoza-Suárez A., Pérez-Aguilar H., Villa-Villa F. (2011), *Optical response of a perfect conductor waveguide that behaves as a photonic crystal*, Prog. Electromagn. Res., **121**, 433–452.
18. Morse P.M., Ingard K.U. (1968), *Theoretical acoustics*, Princeton University Press, USA.
19. Pedersen H.A., Sánches-Sesma F.J., Campillo M. (1994), *Three-dimensional scattering by two-dimensional topologies*, Bulletin of the Seismological Society of America, **84**, 1169–1183.
20. Pérez-Aguilar H., Mendoza-Suárez A., Tututi E., Herrera-Gonzalez I. (2013), *Chaotic behavior of a quantum waveguide*, Physica B, **411**, 93–98.
21. Piscoya R., Ochmann M. (2014), *Acoustical boundary elements: theory and virtual experiments*, Archives Acoustics, **39**, 4, 453–465.
22. Pointer T., Liu E., Hudson J. (1998), *Numerical modelling of seismic waves scattered by hydrofractures: application of indirect boundary element method*, Geophys. J. Int., **135**, 289–303.
23. Tadeu A.J.B., Goginho L., Santos P. (2001), *Performance of the BEM solution in 3D acoustic wave scattering*, Adv. Eng. Soft., **32**, 629–639.
24. Tong M.S., Chew W.C. (2010), *Novel approach for evaluating hypersingular and strongly singular surface integrals in electromagnetics*, IEEE Trans. Antenn. Prop., **58**, 3593–3601.
25. Ursell F. (1973), *On the exterior problems of acoustics*, Proc. Camb. Phil. Soc., **74**, 117–125.
26. Zaman S.I. (2000), *A comprehensive review of boundary integral formulations of acoustic scattering problems*, Sci. Tech. Special Review, pp. 281–310.